Supporting Information

Highly selective synthesis of multi carbon compounds by carbon dioxide hydrogenation over Pt nanocrystals anchoring Ru clusters

Yulv Yu[a†], Yichen Cai[a†], Minghui Liang[b†], Xin Tan[a†], Jin Huang[a], Fukue Kotegawa[c], Zezhou Li[a], Jihan Zhou[a], Masafumi Harada[c]*, Hong Jiang[a]*, Yuan Wang[a]*

[a] Beijing National Laboratory for Molecular Sciences, College of Chemistry and Molecular Engineering, Peking University, Beijing, China.

[b] Key Laboratory of Nanosystem and Hierarchical Fabrication, National Center for Nanoscience and Technology, Beijing, China.

[c] Department of Computer Science and Clothing Environment, Faculty of Human Life and Environment, Nara Women's University, Nara, 630-8506, Japan.

*Corresponding author. E-mail: wangy@pku.edu.cn, harada@cc.nara-wu.ac.jp, h.jiang@pku.edu.cn

Materials and Methods

Materials. Hydrogen (99.999%), carbon dioxide (99.999%) were supplied by Beijing Haikeyuanchang Utility Gas Co., Ltd. $RuCl_3 \cdot nH_2O$ and $H_2PtCl_6 \cdot 6H_2O$ were purchased from Sinopharm Chemical Reagent Co., Ltd. 4,4'-bipyridine (98%) was purchased from Energy Chemical Co., Ltd. Carbon was purchased from Xinsen Carbon Co., Ltd. Cyclohexane of GC grade was purchased from ANPEL Laboratory Technologies (Shanghai) Inc. Other reagents used in this work were of analytical grade. ^{13}C labeled carbon dioxide (purity: 99%) was purchased from Sigma-Aldrich Corporation.

Preparation of catalysts. A glycol solution of NaOH (50 ml, 0.26 M) was added dropwise into a glycol solution of $H_2PtCl_6 \cdot 6H_2O$ (50 ml, 20 g/L) under stirring. The mixture was stirred for 30 minutes and subsequently heated at 160 °C by microwave for 5 minutes under nitrogen atmosphere. A colloidal solution of Pt nanoclusters (Pt: 3.7 g/L) with an average diameter of 1.3 nm was obtained. A colloidal solution of Ru nanoclusters with an average diameter of 1.2 nm (Ru: 3.8 g/L) was prepared using a similar method.

5.9×10^{-3} g of 4, 4'-bipyridine (BIPY) was dissolved in 20 ml of acetone under stirring to prepare a solution. Then, 1 ml of Ru colloidal solution was added dropwise into the solution. The mixture was stirred for 5 h, and a precipitate of BIPY linked Ru NCs was separated by centrifugation which was then re-dispersed in 20 ml of acetone to obtain a suspension. 2 ml of Pt colloid was added dropwise into the suspension. The mixture was subsequently stirred for another 24 h to get the assemblies of Ru and Pt nanoclusters (Ru-bi-Pt). 55 mg of carbon was added into the aforementioned suspension and the mixture was stirred for 24 h at room temperature to prepare carbon supported Ru-bi-Pt (Ru-bi-Pt/C). The mixture was centrifugated to get the solid sample, which was subsequently washed with 40 ml of acetone and dried in a vacuum oven at room temperature. Assemblies of Ru (Ru-bi-Ru) or Pt (Pt-bi-Pt) nanoclusters were prepared using a similar method in the absence of Pt or Ru, respectively, and were subsequently deposited on carbon to prepare Ru-bi-Ru/C and Pt-bi-Pt/C. 200 mg of Ru-bi-Pt/C was dispersed in a mixture of water (5 ml) and cyclohexane (5 ml), and the mixture was sealed in an 15-ml autoclave, to which 1.25 MPa of CO_2 and 3.75 MPa of H_2 were charged and the system was heated at 130 °C for 22 h. Ru-co-Ru/C and Pt-co-Pt/C were prepared by the same method.

Catalyst characterizations. Transmission electron microscope (TEM) characterizations of the samples were performed on an aberration-corrected transmission electron microscope (FEI Titan Cubed Themis G^2 300) with an acceleration voltage of 300 kV. High-angle annular dark filed (HAADF) and elemental distribution images were obtained using scanning transmission electron microscope (STEM) mode. To prepare the TEM samples, the catalysts were dispersed ultrasonically in ethanol for 30 minutes, and then a drop of suspension was placed on a copper grid covered with a carbon film and dried at room temperature overnight.

The in-situ XPS spectra of the samples were collected on ULVAC PHI5000 VersaProbe III. and the transfer vessel was used as the media to transfer the treated sample from the autoclave to the measurement chamber. Before measurements, the samples were pretreated with H_2 in an autoclave at 100 °C for 2 h. After the treatments, the samples were transferred into the transfer vessel using the glove box with oxygen concentration lower than 0.1 ppm. Finally, the samples were transferred from the vessel to the chamber to perform XPS measurements. The binding energy scales for the samples were referenced by setting the C 1s binding energy of contamination carbon to 284.8 eV.

The Pt and Ru contents of catalysts were analyzed by an inductively coupled plasma atomic emission spectrometer (Leeman Corp.).

X-ray absorption fine structure of the samples were measured at High Energy Accelerator Research Organization (KEK, Japan). The EXAFS measurements were conducted in hydrogen atmosphere to avoid the influence of oxygen. The collection of Pt L_{III}-edge spectra was conducted at the beamline 9C of Photo Factory (PF), with an electron storage ring operated at 2.5 GeV and a ring current of 450 mA. Si (111) double crystal monochromator was used for energy selection and higher harmonics elimination was detuned. The collection of Ru K-edge spectra was conducted at the beamline of NW10A of Photon Factory Advanced Ring (PF-AR) with an electron storage ring operated at a 6.5 GeV and a ring current of 55 mA. Si (311) double crystal monochromator was used for energy selection. The ionization chambers with optimized detecting gases [Ar (15%) + N_2 (85%) for incident intensity (I_0), and Ar (100%) for transmitted intensity (I) in Pt L-edge measurements; Ar (100%) for I_0, and Kr (100%) for I in Ru k-edge measurements] were used to acquire radiation intensity. The X-ray energy was scaled with a Pt foil or Ru powder. All XAS and EXAFS data were analyzed by Athena and Artemis program following standard procedures.

Catalytic properties evaluation. Typically, 200 mg of catalyst, 5 ml of water, and 5 ml of cyclohexane were charged in a 15-ml autoclave. The autoclave was sealed and flushed with 1.25 MPa of CO_2 three times to remove the air. Subsequently, 1.25 MPa of CO_2 and 3.75 MPa of H_2 was introduced into the autoclave.

The autoclave was heated to reaction temperatures, and the reactions were carried out under magnetic stirring (1200 rpm). After the reactions, the autoclave was cooled to room temperature with water, and the products were collected for analysis.

In the experiments for testing the stability of Ru-co-Pt/C in CO_2 hydrogenation at 130 °C, the catalyst was recovered by centrifugation, washed with water and cyclohexane, respectively, and used for a new recycling test.

In ^{13}C isotope tracer experiments, 0.75 MPa of ^{13}C labeled carbon dioxide, 2.25 MPa of hydrogen, 200 mg of Ru-co-Pt/C, 5 ml of H_2O and 5 ml of cyclohexane were charged in a 15-ml autoclave, and CO_2 hydrogenation was conducted at 130 °C for 24 h. After the reactions, the products were collected for GC-MS analysis.

Products were identified using gas chromatography (GC) by comparison with authentic samples and gas chromatography-mass spectrometer (GC-MS). The gas mixture was collected with a gas container and analyzed by a GC (Shimadzu GC-2010). The analysis of hydrocarbons in the gas mixture was conducted with an HP-PLOT Q capillary column (ϕ 0.53 mm × 30 m) and a flame-ionization detector (FID). The concentration of CH_4 was analyzed using external normalization method. The concentration of each C_2+ hydrocarbon in the gas mixture was quantified by comparing to CH_4 peak area using response factor as followed:

$$m_{methane} = CVM$$

$$\frac{m_x}{m_{methane}} = \frac{A_x f_x}{A_{methane} f_{methane}}$$

$$n_x = \frac{m_x}{M_X}$$

where C is the measured concentration of methane; V is the volume of the gas mixture; M is the molar mass of methane; x represents a hydrocarbon compound with n carbon numbers; f_x is the response factor of the hydrocarbon; A_x is the measured peak area of the hydrocarbon; and n_x is the mole of the hydrocarbon. CO was analyzed by a CarboPLOT P7 capillary column (ϕ 0.53 mm × 25 m) and a thermal conductivity detector (TCD).

The analysis of hydrocarbons in cyclohexane was conducted with an Rtx-5MS capillary column (ϕ 0.25 mm × 60 m) and an FID. The concentration of decane was analyzed using external normalization method. The concentration of each hydrocarbon in cyclohexane was quantified by comparing with the peak area of decane using response factor as followed:

$$m_{decane} = CVM$$

$$\frac{m_x}{m_{decane}} = \frac{A_x f_x}{A_{decane} f_{decane}}$$

$$n_x = \frac{m_x}{M_X}$$

where C is the measured concentration of decane; V is the volume of cyclohexane; M is the molar mass of decane.

The alcohols in water were analyzed using an HP-INNOWAX capillary column (ϕ 0.32 mm × 30 m) and an FID detector. The concentration of ethanol in water was quantified using external normalization method, and other alcohols were quantified using the methods applied in hydrocarbon quantification.

The mass spectra of hydrocarbons produced in ^{13}C isotope tracer experiments were measured by a Hybrid Quadrupole-Orbitrap GC-MS System (ThermoFisher).

The amount of CO_2 in the gaseous phase was calculated according to the actual gas equation of state using compressibility factor, while that dissolved in cyclohexane and water was calculated according to Henry's law. The yield in a reaction was calculated by the following equation:

$$yield = \frac{\sum_{i=1}^{n} i \times mole\ of\ Ci\ hydrocarbon + \sum_{i=1}^{n} i \times mole\ of\ Ci\ alcohol}{mole\ of\ CO_2\ charged\ in\ the\ system} \times 100\%$$

The selectivity for hydrocarbons or alcohols was calculated by the following equation:

$$Selectivity(Ci) = \frac{i \times mole\ of\ Ci\ hydrocarbon\ (or\ alcohol)}{\sum_{i=1}^{n} i \times mole\ of\ Ci\ hydrocarbon + \sum_{i=1}^{n} i \times mole\ of\ Ci\ alcohol} \times 100\%$$

The average reaction rate ($mol_{CO2} \cdot mol_{metal}^{-1} \cdot h^{-1}$) was calculated based on moles of converted CO_2 and the amount of metal (Ru and Pt) in catalysts.

Density functional theory (DFT) calculations. The global minimum geometry of Ru_{50}, Pt_{50} clusters and Pt_{42}-Ru_8 bimetallic cluster were generated by the ABCluster program,[1] which used artificial bee colony (ABC) algorithm[2] coupled with Gupta potential.[3] A vacuum of 20 Å is added in *z* direction. The DFT calculations were employed by using the Vienna ab initio simulation (VASP) package.[4] The generalized gradient approximation (GGA) Perdew-Burke-Ernzerhof (PBE) functional with spin polarizations was employed to describe the structures and properties.[5] The force convergence was less than 0.03 eV/Å and the energy convergence was 10^{-5} eV for the ion relaxation. The plane-wave basis cutoff was set to 450 eV. The D3 correction of Grimme was added to all calculations.[6] The Γ-centered kpoint Monkhorst-Pack grid was set to be 2 × 2 × 1 for ion relaxation, and a 6 × 6 × 1 k-point was employed for energy calculation. The climbing image NEB method was used to locate transition state of every elementary reaction, and the dimer method was used to continue the calculation for some transition states, which are hard to converge.

Table S1. Catalytic performance of the state-of-the-art catalysts for CO_2 hydrogenation to form multi-carbon compounds.

Catalyst	T	Selectivity (%)				Conversion or yield (%)	Ref.
		CH_4	CO	CH_3OH	C_2^+ compounds (aromatic or paraffin)		
ZnZrO/SAPO	380 ℃	～2%	47%	-	~51%	12.6%	16
ZnAlO/ZSM-5	320 ℃	trace	52%	~1.5%	46.5%	7.5%	21
ZnO-ZrO_2/ZSM-5	340 ℃	trace	34%	-	66%	16%	19
Fe-based	300 ℃	27%	23%	-	50%	19.5%	20
Na-Fe_3O_4/HZSM-5	320 ℃	3.2%	20.1%	-	76.7%	22.0%	17
In_2O_3/HZSM-5	340 ℃	0.6%	44.8%	-	54.6%	13.1%	18
Cr_2O_3/HZSM-5	350 ℃	1.8%	41.2%	-	57.0%	33.6%	22
Co_6/MnO_x	200 ℃	~35%	0.4%	-	~64.6%	15.3%	23
Ru-co-Pt/C	130 ℃	9.6%	-	0.3%	90.1%	8.9%	This work

Fig. S1. HAADF-STEM image of Ru-bi-Pt/C.

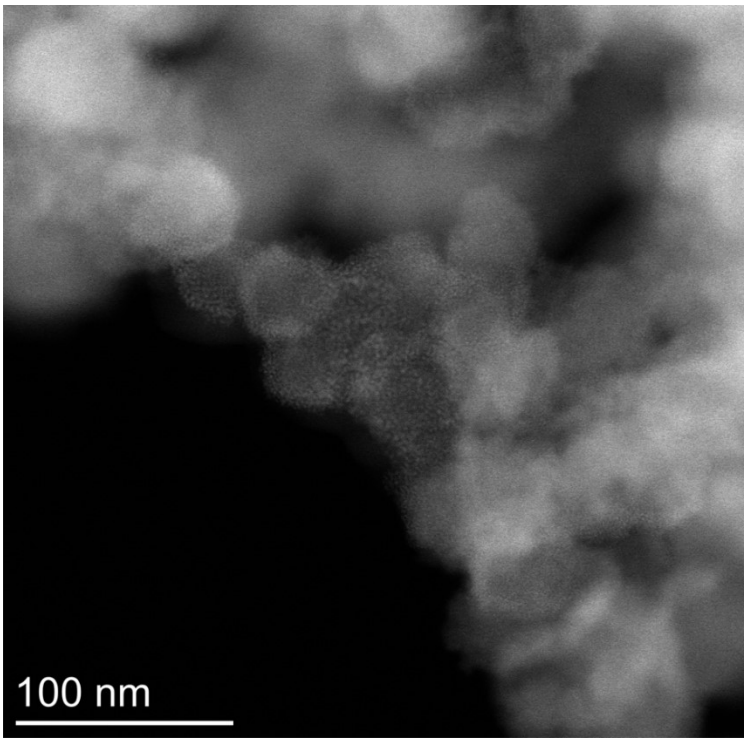

Fig. S2. HAADF-STEM image of Ru-bi-Pt/C (A), and energy dispersive X-ray spectroscopy (EDX) elemental mapping image of Ru (B) and Pt (C) in the selected area. The merged graph (D) of B and C.

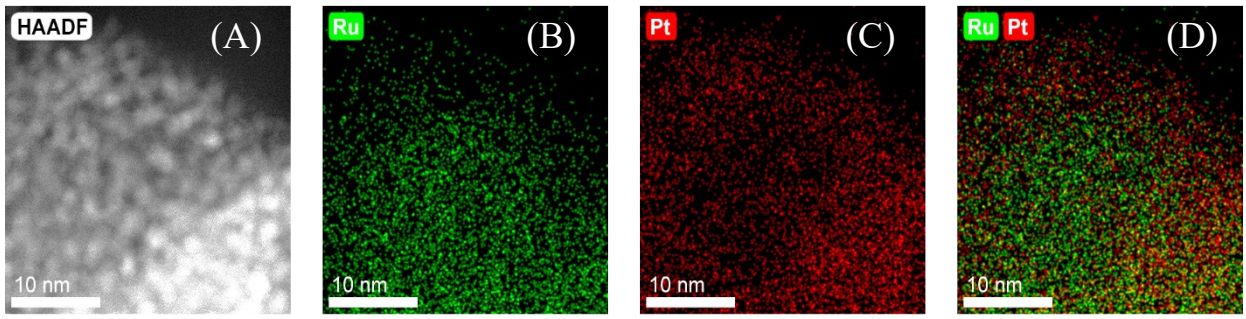

Fig. S3. IR spectrum of Ru-bi-Pt.

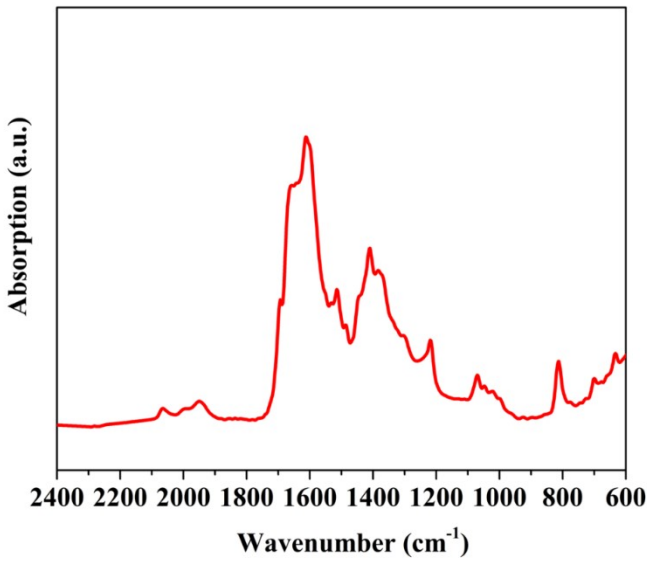

Note: The strong IR absorption bands at 1400~1600 cm^{-1} are assigned to the signals of C=N and C=C stretching in bi-pyridine.

Fig. S4. X-ray photoelectron spectroscopy spectra of Pt 4f (A) and Ru 3p (B) levels in Ru-bi-Pt/C. The binding energy scales for the samples were referenced by setting the C 1s binding energy of contamination carbon to 284.8 eV.

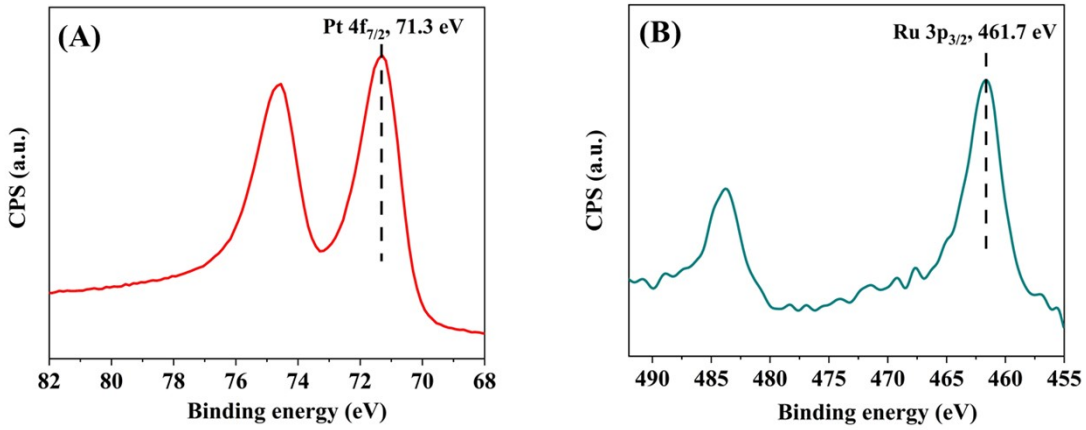

Fig. S5. XPS spectra of N 1s level in Ru-bi-Pt/C and Ru-co-Pt/C, respectively.

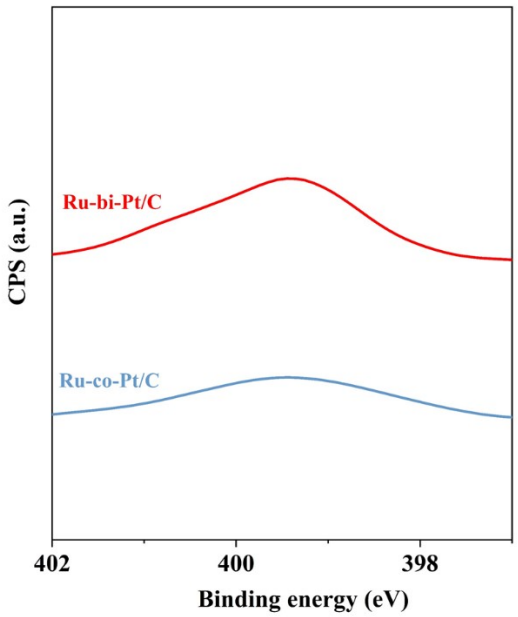

Fig. S6. HAADF-STEM images of Ru-bi-Pt/C (A) and Ru-co-Pt/C (B), and size distributions of metal particles in Ru-bi-Pt/C (C) and Ru-co-Pt/C (D), respectively.

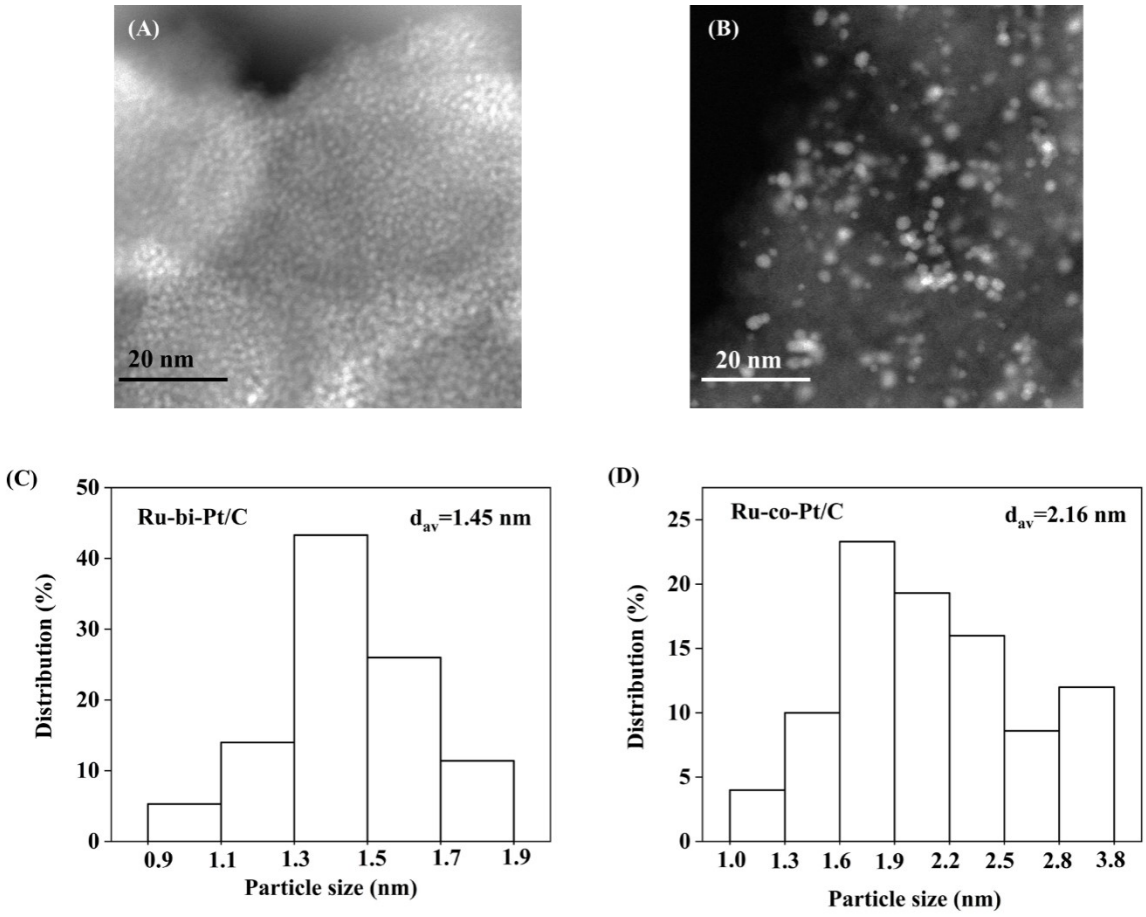

Fig. S7. The EXAFS fitting spectra of Ru-co-Pt/C and Ru-bi-Pt/C at Pt L_3 edge (A, B) and Ru K edge (C, D), respectively.

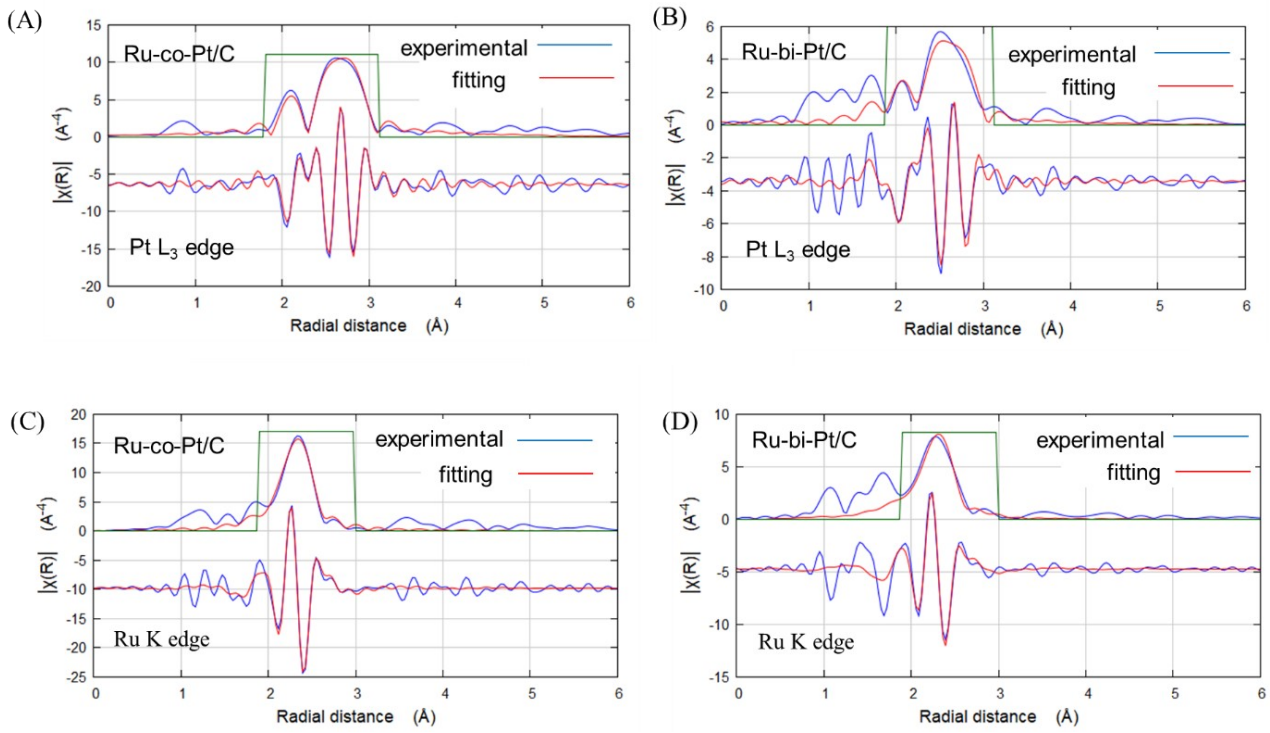

Fig. S8. The HAADF-STEM image (A) of a Pt NC in Pt-co-Pt/C, and line-scan Z-contrast analysis (B, C) of the atom columns along the marked arrow in the Pt NC.

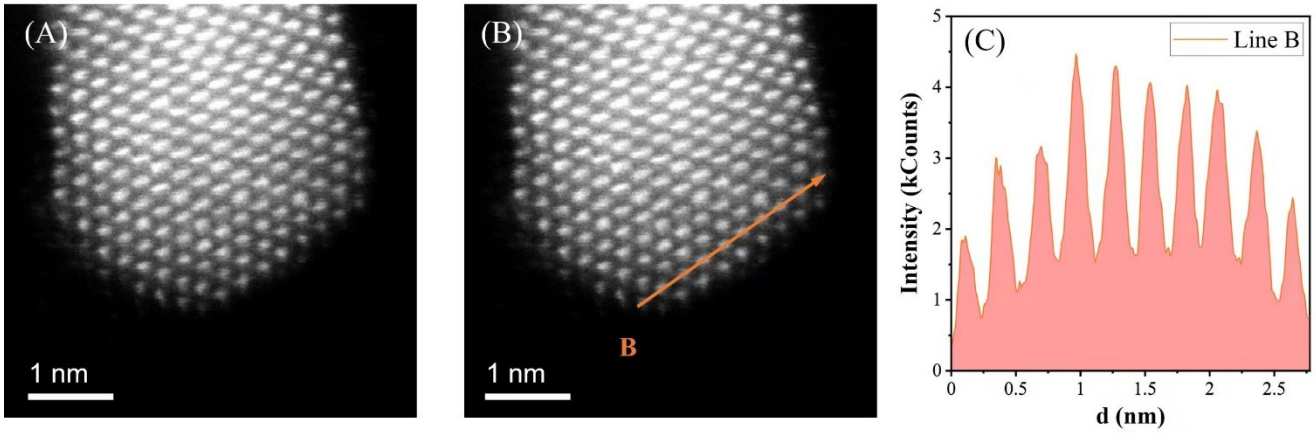

Fig. S9. The HAADF-STEM image of Ru-co-Pt/C. The single atoms on the carbon support were highlighted by circles.

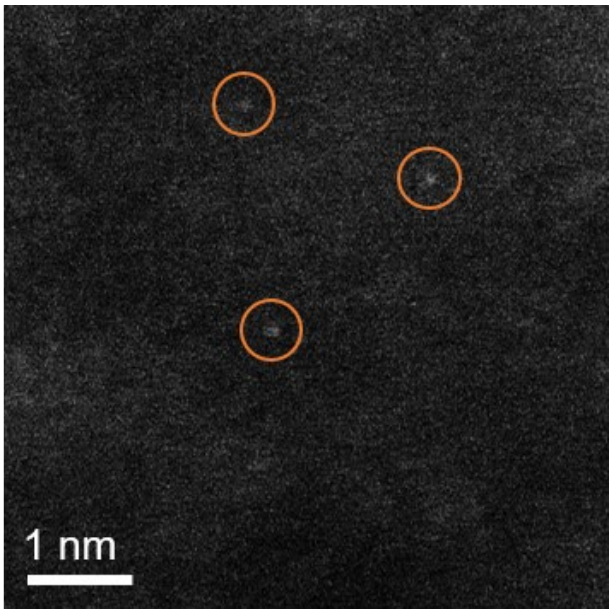

Fig. S10. HAADF-STEM images of Pt-bi-Pt/C (A) and Pt-co-Pt/C (D), EDX elemental mapping image of Pt in Pt-bi-Pt/C (B) and Pt-co-Pt/C (E), and the merged image of A and B (C), and D and E (F).

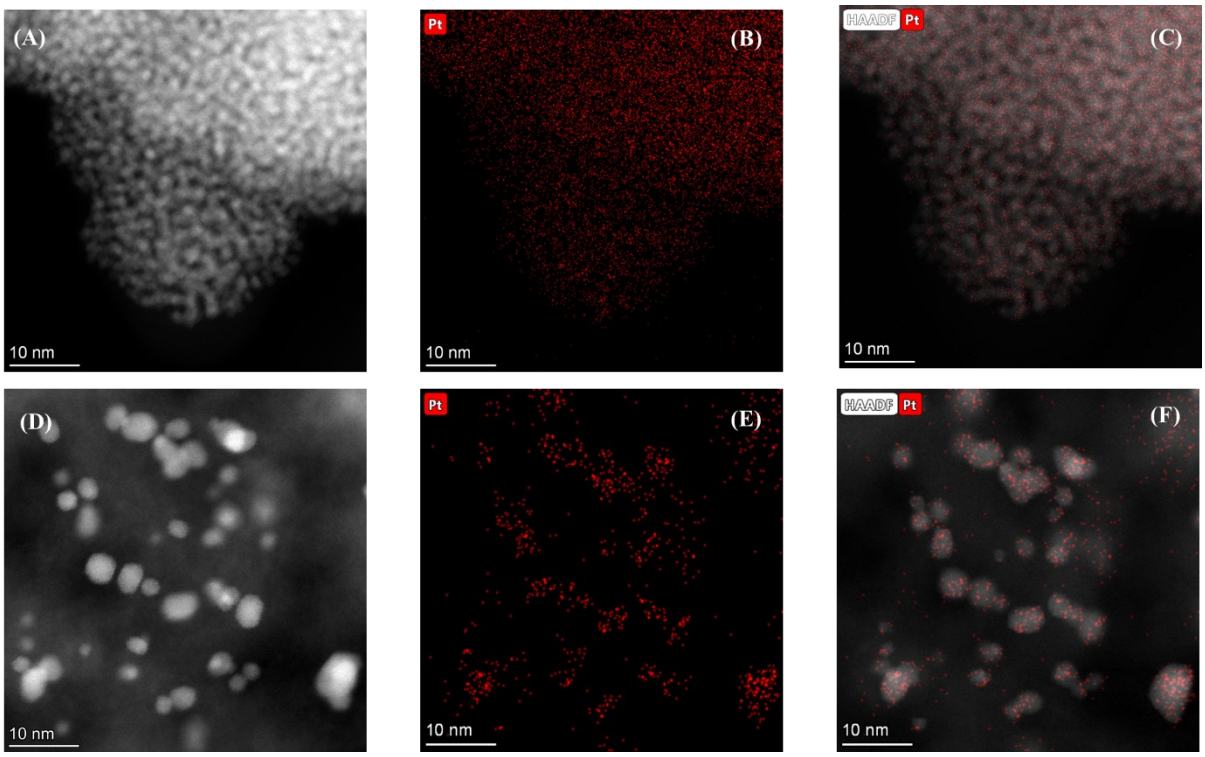

Fig. S11. HAADF-STEM images of Ru-bi-Ru/C (A) and Ru-co-Ru/C (D), EDX elemental mapping image of Ru in Ru-bi-Ru/C (B) and Ru-co-Ru/C (E), and the merged image of A and B (C), and D and E (F).

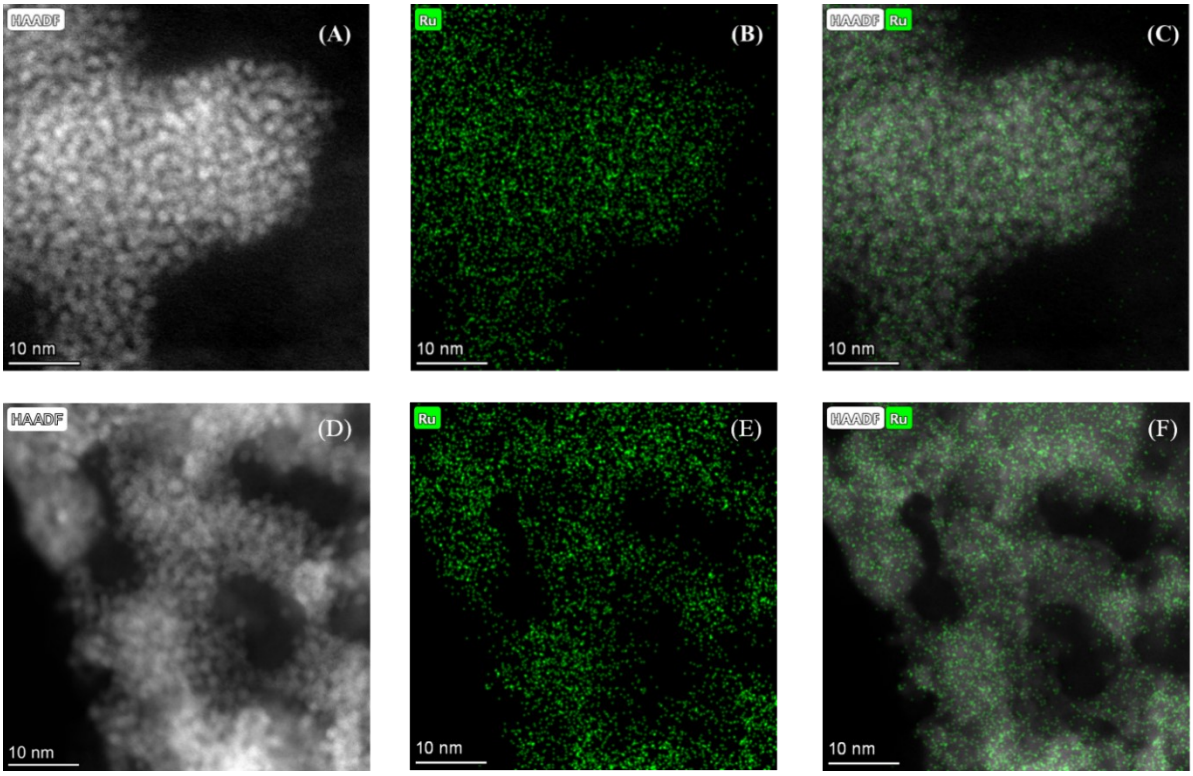

Fig. S12. (A) HAADF-STEM image of the sample obtained by treating Ru-bi-Pt/C with CO_2 under solvothermal conditions. (B) EDX elemental mapping image of Ru and Pt in image A.

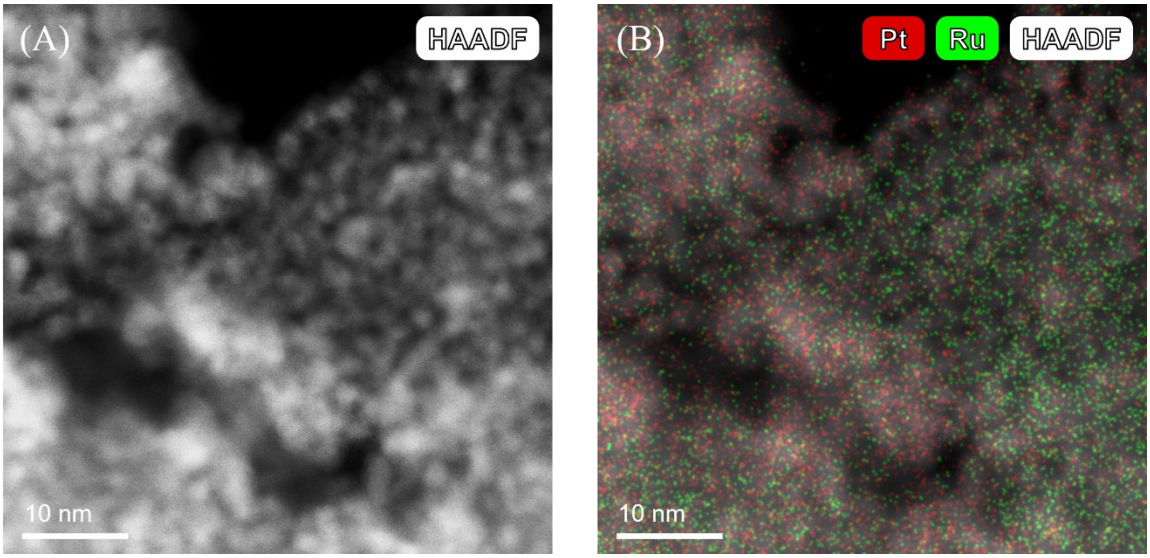

Note: Without H_2 in the reactant atmosphere, the large aggregates of Ru-bi-Pt in Ru-bi-Pt/C could not transform into well dispersed nanoparticles under solvothermal conditions.

Fig. S13. (A) HAADF-STEM image of the sample obtained by treating Ru-bi-Pt/C with H_2 under solvothermal conditions. (B) EDX elemental mapping image of Ru and Pt in image A.

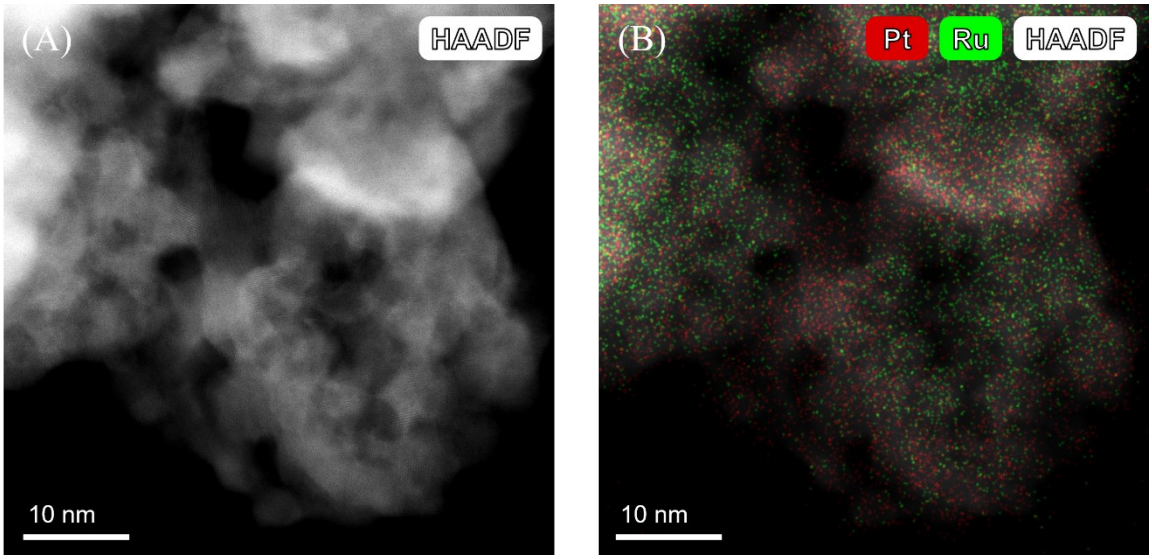

Note: Without CO_2 in the reactant atmosphere, the aggregates of Pt and Ru nanoclusters in Ru-bi-Pt/C fuse to form large bimetallic nanoparticles under solvothermal conditions.

Fig. S14. (A) HAADF-STEM image of spent Ru-co-Pt/C catalyst. (B) EDX elemental mapping image of Ru and Pt in image A. (C) Size distribution of metal particles in the spent Ru-co-Pt/C catalyst.

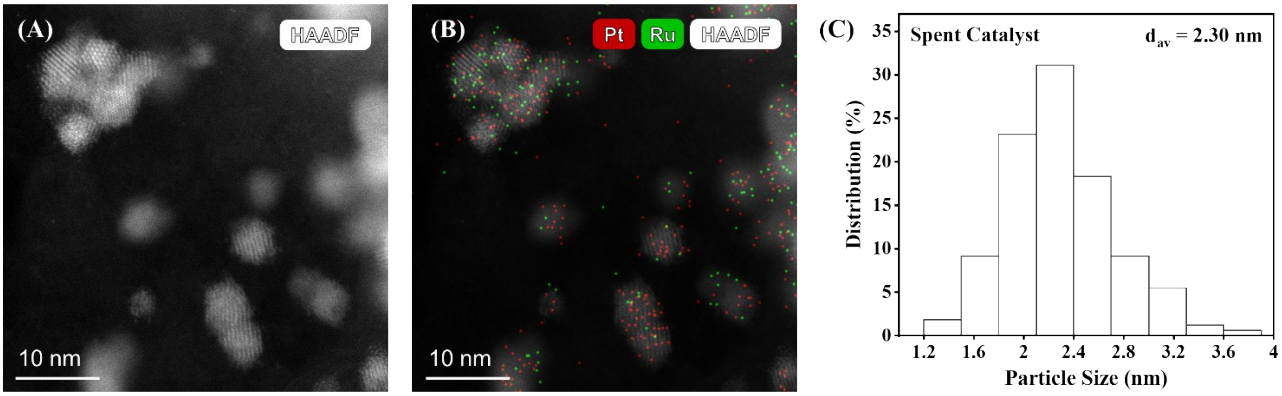

Fig. S15. High resolution mass spectra of $^{13}C_7H_{16}$ (A), $^{13}C_8H_{18}$ (B), and $^{13}C_9H_{20}$ (C) produced in the hydrogenation of ^{13}C labeled carbon dioxide over Ru-co-Pt/C.

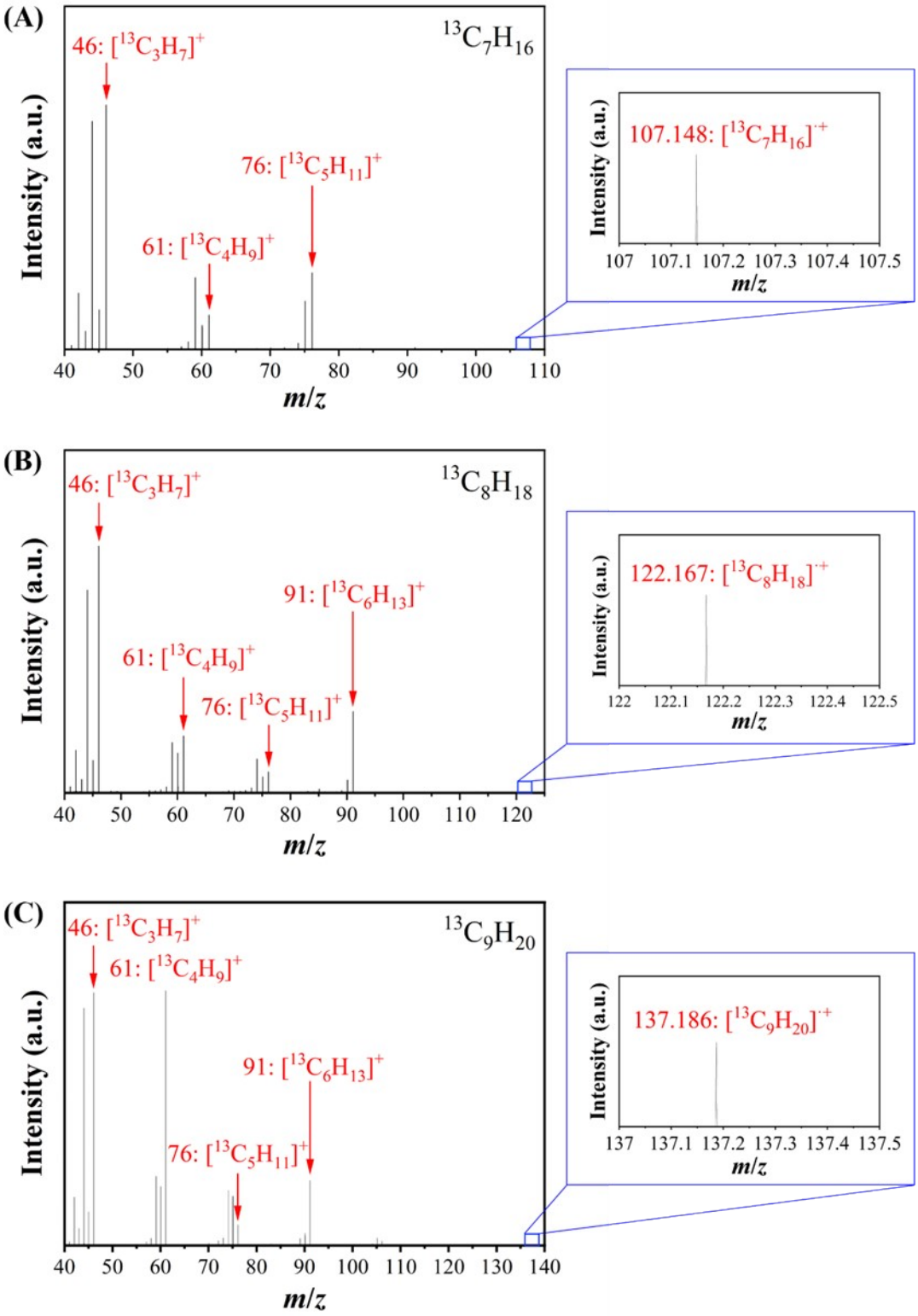

Fig. S16. Top view of Ru_{50} cluster (A), Pt_{50} cluster (C), and Pt_{42}-Ru_8 bimetallic cluster (E). Side view of Ru_{50} cluster (B), Pt_{50} cluster (D), and Pt_{42}-Ru_8 bimetallic cluster (F) in the model catalysts. The green and red balls represent Ru and Pt atom, respectively.

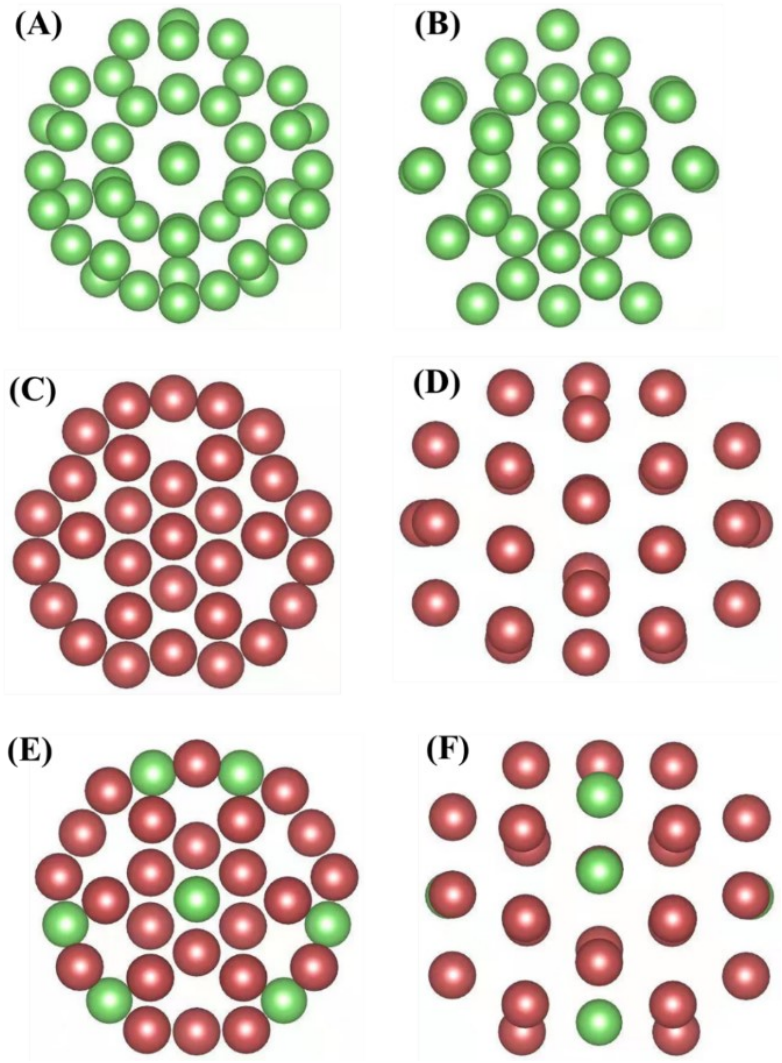

Fig. S17. DFT calculations of energy barriers for CH_2 coupling (A), CH_2 hydrogenation (B), and CH_3 hydrogenation (C) over Ru_{50} nanocluster, respectively. The green, brown, and yellow balls represent Ru, C, and H atom, respectively.

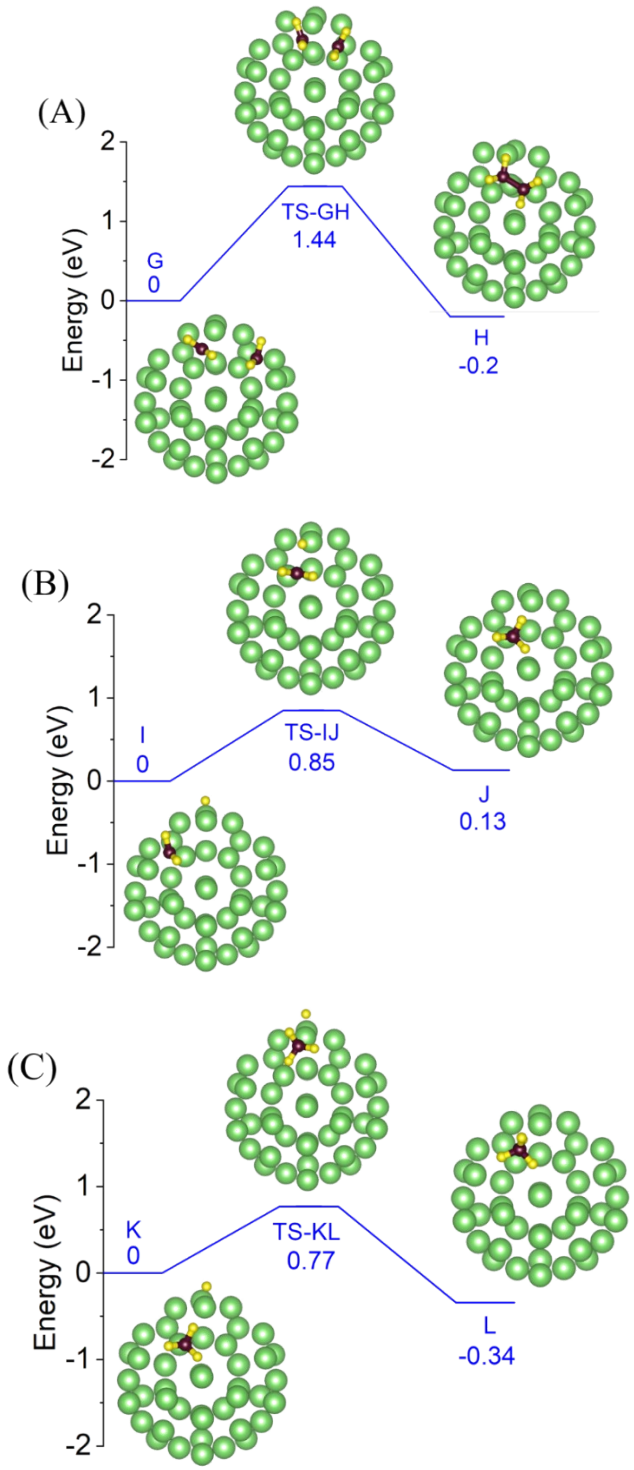

Fig. S18. DFT calculations of energy barriers for CH_2 coupling (A), CH_2 hydrogenation (B), and CH_3 hydrogenation (C) over Pt_{50} nanocluster, respectively. The red, brown, and yellow balls represent Pt, C, and H atom, respectively.

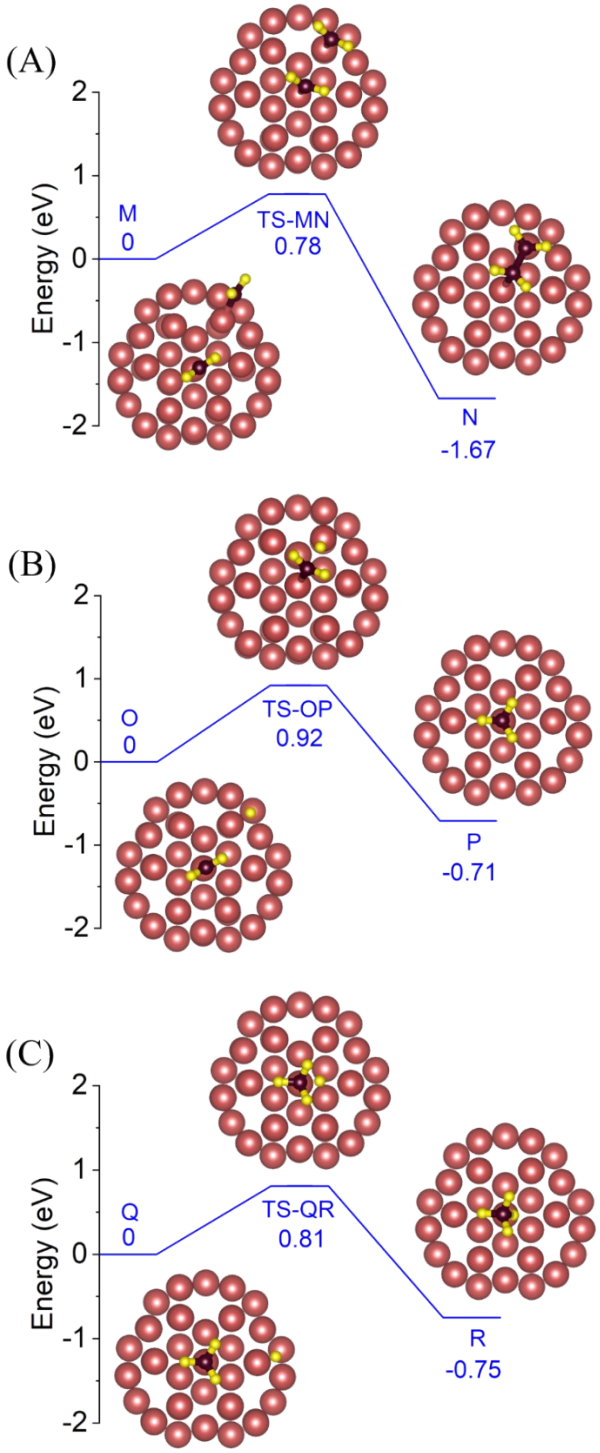

Fig. S19. The optimized structures of CH_2 adsorbed on the (A) Pt site adjacent to Ru_2, and (B) Ru_2 sites in the Pt_{42}-Ru_8 surface, respectively. The red, green, brown, and yellow balls represent Pt, Ru, C, and H atom, respectively.

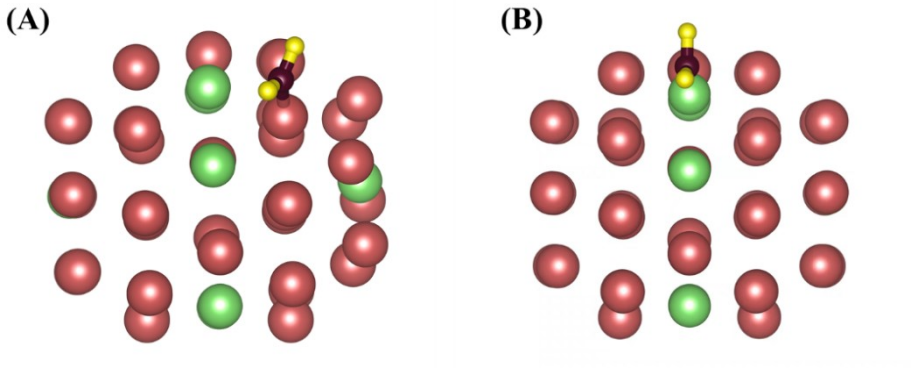

Note: The adsorption energy for CH_2 on the Pt and Ru site was -3.94 and -4.50 eV, respectively.

Fig. S20. The optimized geometries of reactants, transition states and products for CH + CH coupling on Ru_2 in the Pt_{42}-Ru_8 surface. The red, green, brown, and yellow balls represent Pt, Ru, C, and H atom, respectively.

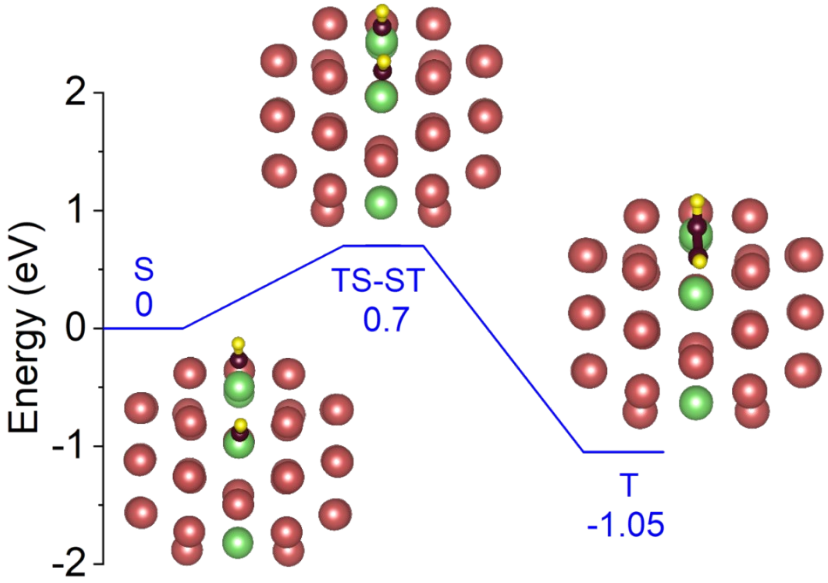

Fig. S21. The optimized structures of H adsorbed on the (A) Pt site adjacent to Ru_2, and (B) Ru_2 sites in the Pt_{42}-Ru_8 surface, respectively. The red, green, and yellow balls represent Pt, Ru, and H atom, respectively.

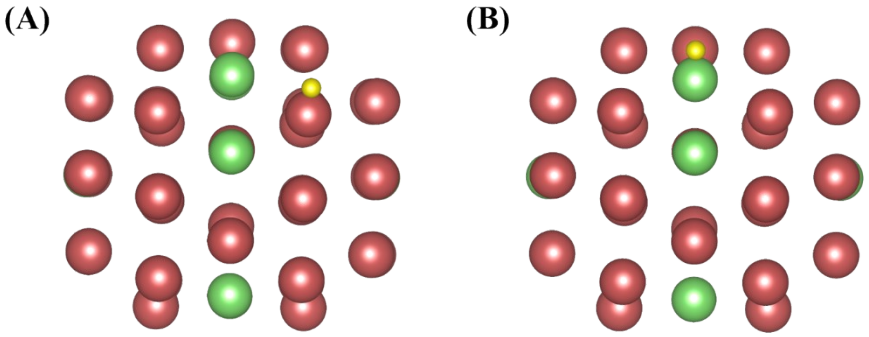

Note: The adsorption energy for H on the Pt and Ru site was -3.02 and -2.84 eV, respectively.

References:

1. J. Zhang, M. Dolg, 2015, *Phys. Chem. Chem. Phys.*, **17**, 24173-24181.

2. J. Zhang, M. Dolg, 2016, *Phys. Chem. Chem. Phys.*, **18**, 3003-3010.

3. R. P. Gupta, 1981, *Phys. Rev. B*, **23**, 6265-6270.

4. G. Kresse, J. Furthmuller, 1996, *Phys. Rev. B*, **54**, 11169-11186.

5. J. P. Perdew, K. Burke, M. Ernzerhof, 1996, *Phys. Rev. Lett.*, **77**, 3865-3868.

6. S. Grimme, S. Ehrlich, L. Goerigk, 2011, *J. Comput. Chem.*, **32**, 1456-1465.